

A Young Stellar Population Around the Intermediate Mass Black Hole ESO 243-49 HLX-1

Sean A. Farrell^{1, 2}, Mathieu Servillat³, Janine Pforr⁴, Thomas J. Maccarone⁵,
Christian Knigge⁵, Olivier Godet^{6,7}, Claudia Maraston⁴, Natalie A. Webb^{6,7}, Didier
Barret^{6,7}, Andrew Gosling⁸, Renaud Belmont^{6,7}, Klaas Wiersema²

¹*Sydney Institute for Astronomy, School of Physics A29, The University of Sydney,
NSW 2006, Australia*

²*Department of Physics and Astronomy, University of Leicester, University Road,
LE1 7RH, Leicester, UK*

³*Harvard-Smithsonian Center for Astrophysics, 60 Garden Street, MS-67,
Cambridge, MA 02138, USA*

⁴*Institute of Cosmology and Gravitation, University of Portsmouth, Dennis Sciama
Building, Burnaby Road, Portsmouth PO1 3FX, UK*

⁵*School of Physics and Astronomy, University of Southampton, Hampshire, SO17
1BJ, UK*

⁶*Université de Toulouse; UPS-OMP; Institut de Recherche en Astrophysique et
Planétologie (IRAP), Toulouse, France*

⁷*CNRS; IRAP; 9 Avenue du Colonel Roche, BP 44346, F-31028 Toulouse Cedex
4, France*

⁸*University of Oxford, Department of Physics, Keble Road, Oxford OX1 3RH, UK*

Intermediate mass black holes with masses between $\sim 100 - 100,000 M_{\odot}$ have important implications for the formation of supermassive black holes (1), cosmology (2,3), and the detection of gravitational wave radiation (4). The recent discovery of ESO 243-49 HLX-1 provides a unique opportunity to

study the environment around an intermediate mass black hole. Here we present *Hubble Space Telescope* and simultaneous *Swift* X-ray telescope observations of HLX-1. The X-ray spectrum is well described by thermal emission from an accretion disc around the black hole. In contrast, the *Hubble* UV, optical and near-infrared data are dominated by emission from a stellar population with an age ~ 6 Myr, implying recent or ongoing interactions between the star cluster containing HLX-1 and the host galaxy ESO 243-49.

The formation of stellar mass black holes (with masses between $\sim 3 - 100 M_{\odot}$) through the collapse of massive stars is well accepted, but it is not yet completely clear how the supermassive black holes found in the centers of most galaxies (with masses between $\sim 10^6 - 10^9 M_{\odot}$) are formed. One possibility is that they are formed from the mergers of intermediate mass black holes with masses in the range of $\sim 10^2 - 10^5 M_{\odot}$ (1). Black holes in this mass range may form in globular clusters (5) or dwarf galaxies (3), with simulations predicting hundreds of isolated (“naked”) intermediate mass black holes populating galaxy halos (6). Intermediate mass black holes are a crucial missing link between stellar mass and supermassive black holes. The existence of intermediate mass black holes also has important implications for other areas of astrophysics including the search for dark matter annihilation signals (predicted to be produced through the compression of dark matter by wandering intermediate mass black holes in galaxy halos; (2)), the epoch of reionisation of the Universe (micro-blazars containing intermediate mass black holes are predicted to have contributed between $\sim 25\%$ – 50% of cosmic reionisation; (3)), and the detection of gravitational wave radiation (from in-spiraling intermediate mass black holes; (4)). The study of intermediate mass black holes

and the environments in which they are found thus has important connotations for a wide range of important questions in modern astrophysics.

The brightest ultra-luminous X-ray source HLX-1 in the edge on early-type S0a galaxy ESO 243-49 currently provides the strongest evidence for the existence of intermediate mass black holes (7). HLX-1 is located in the halo of the galaxy, ~ 0.8 kpc out of the plane and ~ 3.3 kpc away from the nucleus. At the redshift of ESO 243-49 ($z = 0.0223$) the maximum 0.2 – 10 keV X-ray luminosity of HLX-1 is $\sim 1.2 \times 10^{42}$ erg s $^{-1}$ (7), a factor of ~ 400 above the theoretical Eddington limit for a $20 M_{\odot}$ black hole. Luminosities up to $\sim 10^{41}$ erg s $^{-1}$ can be explained by stellar mass black holes undergoing super-Eddington accretion (8) and/or experiencing significant beaming, which makes them appear to exceed the Eddington limit for isotropic radiation (9,10). However, luminosities above $\sim 10^{41}$ erg s $^{-1}$ are very difficult to explain without a more massive black hole. Modelling of the thermal X-ray emission of HLX-1, using a relativistic disc model (assuming a Shakura-Sunyaev disc structure) has shown that it is consistent with an accretion disc around a black hole with a mass between $\sim 3,000 - 100,000 M_{\odot}$ (11). This mass range is also consistent with mass estimates obtained from Eddington scaling that implies a mass $> 9,000 M_{\odot}$ assuming a standard disc (12).

Using X-ray observations with *Chandra*, we localised the position of HLX-1 to sub-arcsecond accuracy (13) resulting in the discovery of a faint optical counterpart with $R \sim 24$ mag (14). The distance and thus the luminosity were subsequently confirmed through the detection of the H α emission line at a redshift consistent with the host galaxy (15). An excess of UV emission was also detected near the position of HLX-1 with the *GALEX* and *Swift* observatories, although the angular

resolution of these telescopes was not sufficient to cleanly distinguish any emission from that of the nucleus of ESO 243-49 (13). At least some of this UV emission is likely to be associated with a background galaxy at a redshift of $z \sim 0.03$ that was detected $\sim 3''$ from HLX-1 in Very Large Telescope spectroscopy (15, 16).

A long-term monitoring campaign with the *Swift* observatory has shown that the 0.2 – 12 keV luminosity of HLX-1 varies by a factor of ~ 50 from $\sim 2 \times 10^{40} - 1 \times 10^{42} \text{ erg s}^{-1}$, with correlated spectral variability reminiscent of the spectral hysteresis behaviour observed in Galactic stellar mass black hole (12). Since the *Swift* monitoring began in 2009, HLX-1 has been observed to undergo three outbursts, each spaced approximately one year apart (12). The timescales and amplitude of the outbursts are not consistent with the thermal-viscous disc instability model, leading to the conclusion that the outburst mechanism could be driven by tidal stripping of a companion star in an eccentric orbit during periastron passage (17). Constraining the environment around HLX-1 therefore has important implications for the nature of any companion star.

Following the peak of the second outburst we obtained three orbits of observations with the *Hubble Space Telescope (HST)* on the 13th and 23rd of September 2010 in order to constrain the nature of the environment around HLX-1. The *HST* is crucial for broadband studies of objects such as HLX-1 due to its broad wavelength range covering UV to near-infrared bands and an angular resolution that allows efficient removal of the host galaxy light. These observations were performed with the Advanced Camera for Surveys (ACS) and Wide Field Camera 3 (WFC3) instruments in six filters covering near-infrared (F160W filter), optical (F774W, F555W, and F390W filters), and UV (F300X and F140LP filters)

wavelengths. A single point source was significantly detected in all the images within the 95% confidence levels of the combined *Chandra* and *HST* astrometry (Figure 1). The source was unresolved, giving an upper limit of ~ 60 pc on the size of the counterpart at the distance to HLX-1 of 95 Mpc (18).

Simultaneous X-ray data were taken with the *Swift* X-ray telescope (XRT). The X-ray spectrum is consistent with both thermal and non-thermal emission and an acceptable fit was obtained with multi-coloured disc black body and power law models. However, a deeper X-ray spectrum obtained with *Chandra* just one week prior to the first of the *HST* orbits found that the spectrum was inconsistent with non-thermal emission, and that HLX-1 was in the thermally dominated high/soft spectral state (12). We therefore adopt thermal models for the fitting to the X-ray part of the Spectral Energy Distribution (SED). Fitting the near-infrared to X-ray SED with simple disc models identified the presence of a significant red excess in the *HST* bands. Adopting a model that includes reprocessing of the outer accretion disc improved the fit, but not to a statistically acceptable level ($\chi^2/dof = 56.21/30$).

The residuals indicated a problem with the fit in the blue *HST* bands, and so we added a model component representing emission from a stellar population using the theoretical integrated spectral energy distributions of stellar population models by (19), with no priors imposed on the age or metallicity. The observed SED was found to be consistent with a model comprised of a minimally irradiated accretion disc with the addition of emission from a young stellar population ($\chi^2/dof = 25.18/27$). Model components representing dust extinction and neutral hydrogen column absorption were included in the fits, obtaining values slightly above the Galactic values in the direction of HLX-1. The fraction of bolometric

luminosity that is reprocessed in the outer disc was poorly constrained, and so a solution where a significant amount of disc irradiation is present is also allowed (with the luminosity and therefore mass of the stellar component a factor of ~ 10 higher). We therefore cannot determine whether or not significant irradiation of the outer disc is present with the available data. However, irrespective of whether irradiation was included or not, the age of the stellar population was consistently found to be young. Table 1 lists the spectral parameters for the best-fit model with minimum irradiation, Figure 2 shows the SED fitted with this model, and Figure 3 shows the de-reddened and unabsorbed model. Using the stellar population models by (20), which are based on empirical stellar libraries, also obtained an excellent fit ($\chi^2/dof = 27.32/28$) with consistent model parameter values.

The age of the stellar population was found to be 6.3 Myr. The free model parameters for the irradiated disc component all fall within the physical range expected for an intermediate mass black hole, with the inner disc temperature of 0.18 keV being consistent with previous measurements (7, 11, 12). Assuming a non-spinning black hole and that the system angle of inclination lies between $\sim 0^\circ - 60^\circ$ (based on the lack of evidence for eclipses in the X-ray light curve), we estimated the black hole mass to be $\sim 20,000 M_\odot$, consistent with previous estimates (11, 12) and clearly within the intermediate mass range. The upper limit on the outer radius of the accretion disc could not be constrained, but the best-fit value indicates an outer radius of ~ 8 AU.

The detection of a stellar population around HLX-1 provides intriguing insights into the origin of and environment around an intermediate mass black hole. Possible environments for the formation of intermediate mass black holes include

globular clusters (5) and the nuclei of dwarf galaxies (3). Globular clusters are dense clusters of stars that are found in the halos of many galaxies, including the Milky Way. The high concentration of stars results in a large probability of interactions, creating a natural environment for mergers and rapid accretion. Thus, a black hole forming in a globular cluster could potentially grow rapidly to a mass of around $20,000 M_{\odot}$. Alternatively, if dwarf galaxies contain nuclear black holes and if the black hole mass scales with the mass of the galaxy bulge (as it does with higher mass galaxies), then the nuclear black holes would be expected to be intermediate mass (21). Interactions between a dwarf satellite galaxy and the larger host galaxy could strip away most of the mass of the dwarf galaxy, leaving behind a compact star cluster surrounding the black hole. Such interactions are likely to drive star formation in this cluster and could also trigger accretion, producing X-ray emission at luminosities in the ULX range. However, the X-ray variability observed from HLX-1 argues against direct accretion from material funnelled down onto the black hole following a merger event, and instead implies the presence of a binary companion.

The results of the SED fitting indicate that young massive stars dominate the optical emission from the stellar cluster around HLX-1. Such a young stellar population is difficult to reconcile with HLX-1 residing in a classical globular cluster, such as those observed in our own Galaxy that are typically dominated by old stars. However, young globular clusters with young stellar populations have been observed around disrupted galaxies such as the Antennae galaxies (22). The mass of the cluster around HLX-1 (calculated using the derived age and metallicity, the

observed luminosity and the model mass-to-light ratio¹) is $\sim 2 \times 10^6 M_{\odot}$, which is at the upper end of the standard classical globular cluster mass range (23). If the level of irradiation is higher than obtained from the best fit to the SED then the luminosity and mass of the stellar population are lowered to $\sim 8 \times 10^7 L_{\odot}$ and $\sim 4 \times 10^5 M_{\odot}$, respectively, well within the normal range of globular cluster masses.

The presence of a young stellar population surrounding HLX-1 could also be explained in the accreted dwarf galaxy scenario (24). Tidally stripping a dwarf galaxy during a merger event could remove a large fraction of the mass from the dwarf galaxy, with star formation triggered as a result of the tidal interactions. This could result in the observed intermediate mass black hole embedded in the remnant of the nuclear bulge with a young, high metallicity, stellar population. It has been proposed that such accreted dwarf galaxies may explain the origin of globular clusters, with the remnant cluster appearing more like a classical globular cluster as its stellar population ages. This scenario has been proposed to explain the origin of some Galactic globular clusters and may explain the origin of a significant number of the globular clusters in a given galaxy (25). Thus, we cannot distinguish between a globular cluster and a nucleated dwarf galaxy using the spectral fitting. However, it would be hard to form a young globular cluster outside the disc of the galaxy, and so we favour the nucleated dwarf galaxy scenario.

A link has been drawn between the presence of prominent dust lanes in early-type galaxies with frequent gas-rich minor mergers (i.e. interactions with lower

¹ See <http://www.maraston.eu>

mass dwarf galaxies), with the host galaxy nuclear black hole becoming active within < 200 Myr following the merger event (26). The *HST* images of ESO 243-49 reveal pronounced dust lanes and yet no evidence of nuclear activity was detected in *Chandra* X-ray images (12) implying that the merger events that contributed to the formation of the dust lanes took place in the recent past. This is thus consistent with the presence of a young stellar population surrounding HLX-1. This young star cluster is likely the product of localised star formation triggered as a result of tidal interactions with ESO 243-49 following a recent merger event, in the context of a recently formed globular cluster and/or an accreted dwarf galaxy.

References:

1. M. Fornasa, G. Bertone, Black holes as dark matter annihilation boosters. *Int. J. Mod. Phys. D.* **17**, 1125-1157 (2008).
2. M. Ricotti, J. P. Ostriker, X-ray pre-ionization powered by accretion on the first black holes - I. A model for the WMAP polarization measurement. *Mon. Not. R. Astron. Soc.* **352**, 547-562 (2004).
3. B. P. Abbott *et al.*, Search for gravitational wave ringdowns from perturbed black holes in LIGO S4 data. *Phys. Rev. D.* **80**, 062001 (2009).
4. T. Ebisuzaki *et al.*, Missing link found? The “runaway” path to supermassive black holes. *Astrophys. J.* **562**, L19-L22 (2001).
5. M. C. Miller, D. P. Hamilton, Production of intermediate-mass black holes in globular clusters. *Mon. Not. R. Astron. Soc.* **330**, 232-240 (2002).
6. J. M. Bellovary *et al.*, Wandering black holes in bright disk galaxy halos. *Astrophys. J.* **721**, L148-L152 (2010).
7. S. A. Farrell, N. A. Webb, D. Barret, O. Godet, J. M. Rodrigues, An intermediate-mass black hole of over 500 Solar masses in the galaxy ESO 243-49. *Nature.* **460**, 73-75 (2009).
8. M. C. Begelman, Super-Eddington fluxes from thin accretion disks? *Astrophys. J.* **568**, L97-100 (2002).
9. A. R. King, Accretion rates and beaming in ultraluminous X-ray sources. *Mon. Not. R. Astron. Soc.* **385**, L113-L115 (2008).

10. M. Freeland, Z. Kuncic, R. Soria, G. V. Bicknell, Radio and X-ray properties of relativistic beaming models for ultraluminous X-ray sources. *Mon. Not. R. Astron. Soc.* **372**, 630-638 (2006).
11. S. W. Davis *et al.* The cool accretion disk in ESO 243-49 HLX-1: further evidence of an intermediate-mass black hole. *Astrophys. J.* **734**, 111 (2011).
12. M. Servillat *et al.* X-ray variability and hardness of ESO 243-49 HLX-1: clear evidence for spectral state transitions. *Astrophys. J.*, in press (available at <http://arxiv.org/abs/1108.4405>).
13. N. A. Webb *et al.* Chandra and Swift follow-up observations of the intermediate-mass black hole in ESO 243-49. *Astrophys. J.* **712**, L107-L110 (2010).
14. R. Soria *et al.* Discovery of an optical counterpart to the hyperluminous X-ray source in ESO 243-49. *Mon. Not. R. Astron. Soc.* **405**, 870-876 (2010).
15. K. Wiersema *et al.* A redshift for the intermediate-mass black hole candidate HLX-1: confirmation of its association with the galaxy ESO 243-49. *Astrophys. J.* **721**, L102-L106 (2010).
16. S. A. Farrell *et al.* Exploring the nature of the brightest hyper-luminous X-ray source. *Astronomische Nachrichten.* **332**, 392-397 (2011).
17. J.-P. Lasota *et al.* The origin of the variability of the intermediate-mass black-hole ULX system HLX-1 in ESO 243-49. *Astrophys. J.* **735**, 89 (2011).
18. Materials and methods are available as supporting material on *Science Online*.
19. C. Maraston, Evolutionary population synthesis: models, analysis of the ingredients and application to high-z galaxies. *Mon. Not. R. Astron. Soc.* **362**, 799-825 (2005).
20. C. Maraston, G. Stromback, Stellar population models at high spectral resolution. *Mon. Not. R. Astron. Soc.*, in press (available at <http://arxiv.org/abs/1109.0543>).
21. J. E. Greene, L. C. Ho, A new sample of low-mass black holes in active galaxies. *Astrophys. J.* **670**, 92-104 (2007).
22. N. Bastian, E. Emsellem, M. Kissler-Patig, C. Maraston, Young star cluster complexes in NGC4038/39. Integral field spectroscopy using VIMOS-VLT. *Astron. Astrophys.* **445**, 471-483 (2006).
23. C. Maraston *et al.*, The dynamical mass of the young cluster W3 in NGC 7252. Heavy-weight globular cluster or ultra compact dwarf galaxy? *Astron. Astrophys.* **416**, 467-473 (2004).
24. K. A. Knieperman, in *Galaxy Wars: Stellar Populations and Star Formation in Interacting Galaxies*, B. Smith, N. Bastian, S. Higdon, J. Higdon, Eds. (ASPC, San Francisco, 2010), pp. 342-345.
25. D. A. Forbes, T. Bridges, Accreted versus in situ Milky Way globular clusters. *Mon. Not. R. Astron. Soc.* **404**, 1203-1214 (2010).

26. S. S. Shabala *et al.*, Galaxy Zoo: dust lane early-type galaxies are tracers of recent, gas-rich minor mergers. *Mon. Not. R. Astron. Soc.*, submitted (available at <http://arxiv.org/abs/1107.5310>).
27. N. Zacharias *et al.*, The third US naval observatory CCD astrograph catalog (UCAC3). *Astron. J.* **139**, 2184-2199 (2010).
28. N. S. van der Bliek *et al.*, ISPI: a wide-field NIR imager for the CTIO Blanco 4-m telescope. *Proc. SPIE.* **5492**, 1582-1589 (2004).
29. K. Lodders, Solar system abundances and condensation temperatures of the elements. *Astrophys. J.* **591**, 1220-1247 (2003).
30. M. Gierlinksi, C. Done, K. Page, Reprocessing of X-rays in the outer accretion disc of the black hole binary XTE J1817-330. *Mon. Not. R. Astron. Soc.* **392**, 1106-1114 (2009).
31. A. J. Pickles, A stellar spectral flux library: 1150-25000 Å. *Publ. Astron. Soc. Pac.* **110**, 853-878 (1998).

Supporting Online Material

www.sciencemag.org

Materials and Methods

Tables S1, S2

References (

Acknowledgements

We thank C. Done, S. Shabala, F. Grisé, K. Arnaud and R. Starling for helpful interactions. SAF is the recipient of an Australian Research Council Postdoctoral Fellowship, funded by grant DP110102889. SAF, TJM, AJG and KW acknowledge funding from the UK Science and Technology Funding Council. MS acknowledges support from NASA/Chandra grants GO0-11063X, DDo-11050X and NSF grant AST0909073. JP and CM acknowledge the Marie-Curie Excellence Team grant 'Unimass', ref. MEXT-CT-2006-042754 of the Training and Mobility of Researchers programme financed by the European Community. TJM thanks the European Union FP7 for support through grant 215212 Black Hole Universe. Based on observations made with the NASA/ESA Hubble Space Telescope, obtained at the Space Telescope Science Institute, which is operated by the Association of Universities for Research in Astronomy, Inc., under NASA contract NAS 5-26555. These observations are associated with program #12256. Also based on observations with Swift, launched in November 2004, is a NASA mission in partnership with the Italian Space Agency and the UK Space Agency.

Table 1 Best fit SED model parameters

Parameter	Value	Unit
Extinction, E(B-V)	$0.47^{+0.04}_{-0.1}$	mag
Absorption, nH	$0.13^{+0.01}_{-0.01}$	10^{22} atoms cm^{-2}
Metallicity of stellar population, Z	$2.0^{+0}_{-0.08}$	Z_{\odot}
Age of stellar population	$6.3^{+0.1}_{-0.2}$	10^6 yr
Inner disc temperature, kT_{DISC}	$0.18^{+0.01}_{-0.01}$	keV
Compton slope, Γ	2.1 (fixed)	
High energy rollover temperature, kT_{E}	100 (fixed)	keV
Compton to disc luminosity ratio, $L_{\text{C}}/L_{\text{D}}$	$0.08^{+0.04}_{-0.04}$	
Compton thermalisation fraction, f_{IN}	0.0 (fixed)	
Compton illuminated disc radius, r_{IRR}	1.001 (fixed)	R_{in}
Thermalised bolometric flux fraction, f_{OUT}	$2^{+3000}_{-2} \times 10^{-5}$	
Outer disc radius, $\text{Log}(r_{\text{OUT}})$	4^{+0}_{-1}	$\text{Log}(R_{\text{in}})$
χ^2 / dof	25.18/27	
Bolometric luminosity of stellar population, L_{SSP}	1.3×10^{42}	erg s^{-1}
	3.4×10^8	L_{\odot}
Mass of stellar population, M_{SSP}	2×10^6	M_{\odot}
Bolometric luminosity of accretion disc, L_{DISKIR}	2.3×10^{42}	erg s^{-1}

The slope of the power law photon index of the Comptonisation component could not be constrained and was frozen at a value of 2.1. Likewise, the fraction of luminosity in the Compton tail which is thermalised in the inner disc (f_{IN}) was frozen at 0 and the radius of the Compton illuminated disc (r_{IRR}) was frozen at 1.001, as the Compton tail is not dominant in the disc-dominated state. The upper uncertainties of the stellar population metallicity and the outer disc radius could not be constrained. All errors quoted are at the 95% confidence level.

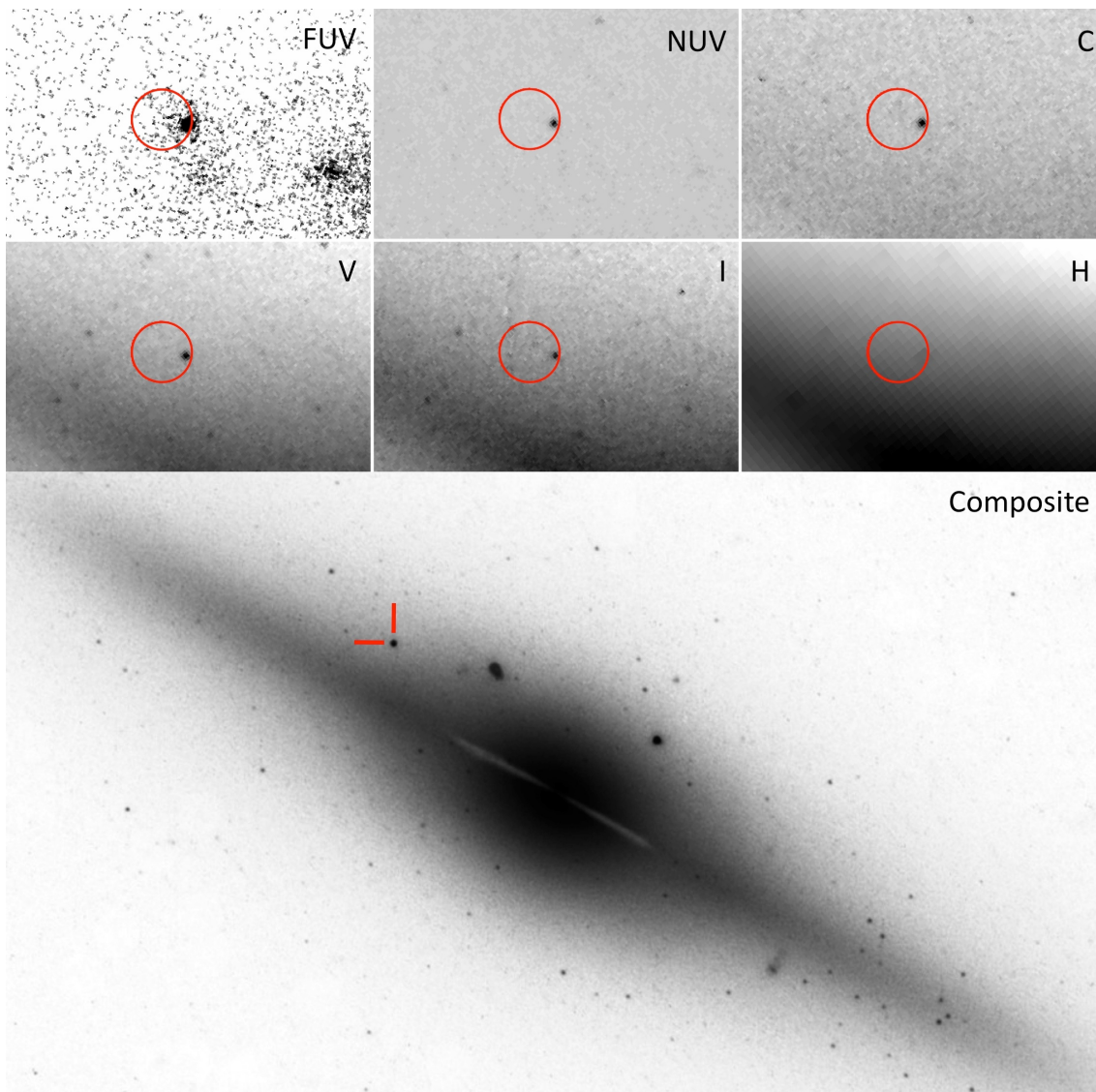


Figure 1 | *HST* images of HLX-1. Top: images from each of the 6 filters (far-UV, near-UV, Washington C-band, V-band, I-band, and H-band) zoomed in on the position of HLX-1. The circles indicate the X-ray position of HLX-1 with the radii of 0.5" indicating the combined *HST* plus *Chandra* 95% astrometric error. Bottom: combined image constructed from all images, showing the prominent dust lanes in the nucleus of ESO 243-49. The position of the HLX-1 counterpart is indicated by the tick marks. In all images North is up and East is left.

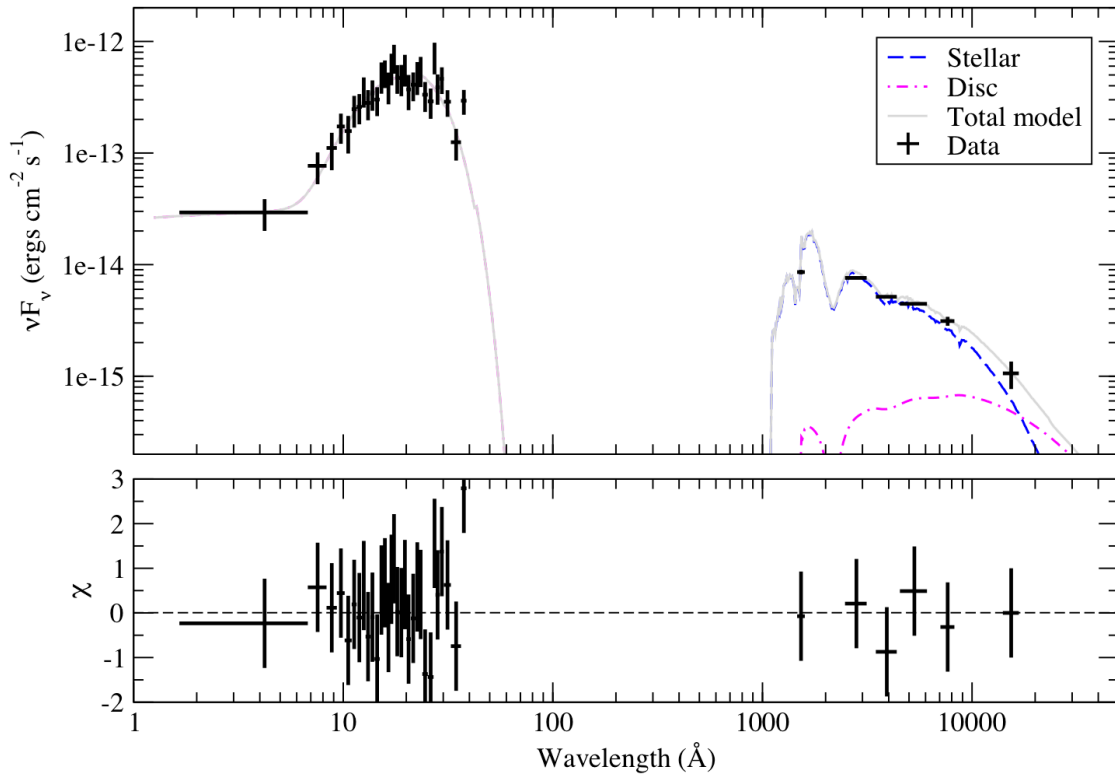


Figure 2 | Best-fit broadband SED model of HLX-1. Top: the *Swift* XRT (left) and *HST* (right) data points fitted with a non-irradiated disc plus young stellar population model. Bottom: residuals to the fit.

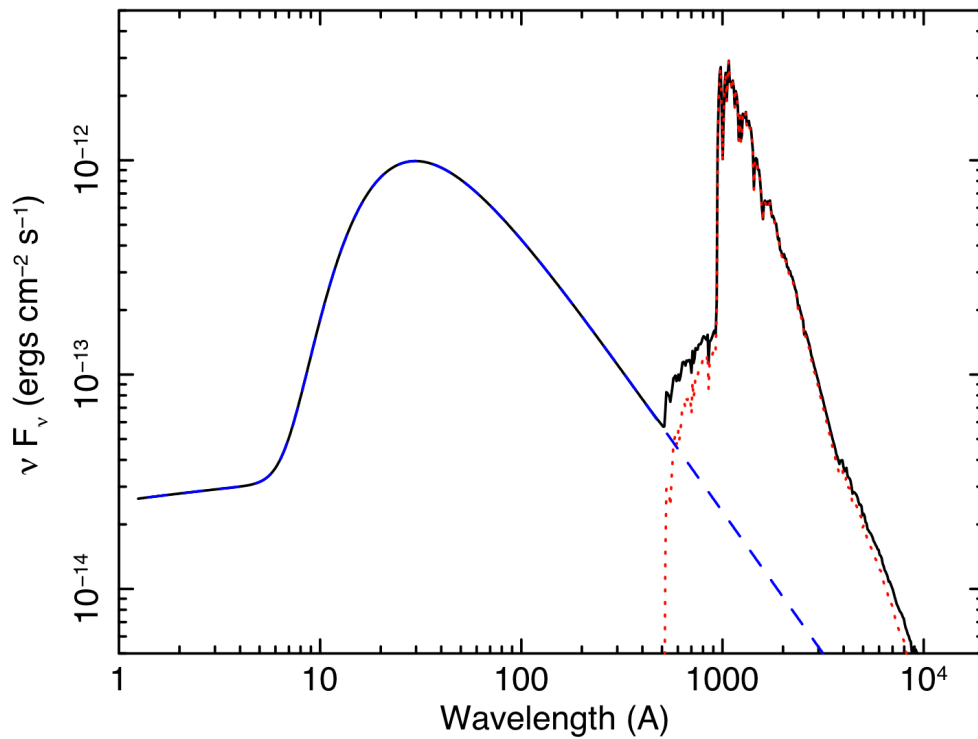


Figure 3 | De-reddened and unabsorbed best-fit SED model. Below ~ 500 Å the SED is dominated by an irradiated accretion disc (blue dashed line), with the spectrum above this wavelength dominated by a young stellar population (red dotted line). The black solid line indicates the combined model.

Supporting Online Material

HST Data Reduction & Analysis

Table S1 presents the log of the *HST* observations, which were observed under program #12256. We analyzed the final *HST* images generated by the pipeline (drz files) using the latest calibration data (CALWF3=2.1 as of 15-May-2010, and CALACS=5.1.1 as of April 27 2010). During the pipelined process, those images were flat fielded, combined (with cosmic ray rejection) and undistorted using PyDrizzle v6.3.5 (May 19 2010).

Astrometry

We corrected the astrometry of each HST image following a two-step procedure with an intermediate image and using the UCAC3 catalogue (27) as an astrometric reference (typical rms error of 0.1"). As the HST WFC3 and ACS fields of view are relatively small and the target is located in a particularly empty field that contains 1 or 2 UCAC3 sources only (including the extended source ESO 243-49 itself), we used an intermediate image obtained with ISPI at CTIO (28) on 2009 August 2. This image covers a 10' x 10' region around ESO 243-49 in the J-band. We aligned the ISPI image on the UCAC3 catalogue with Starlink/GAIA and obtained a precision of 0.13" (rms) based on 9 reference stars. We then used the ISPI image as a reference to align the WFC3 images. The number of stars used in the process and the resulting absolute position error are given in Table S2 for each band. For the ACS/SBC image (F140LP filter), this process could not be applied because of the lack of detection of ISPI stars in this band. We thus used the WFC3/UVIS NUV image as a reference and found 5 common objects. The precision is also reported in Table S2. The position of the X-ray source HLX-1 is 0.3" at 95% confidence. The

final position error, adding in quadrature all errors, is thus below 0.5" at 95% confidence level for each Hubble image. This error circle is reported in Figure 1 and a single counterpart is clearly detected in each band (in the F160W H-band filter it is difficult by eye to see the counterpart amongst the strong diffuse emission from the galaxy, but a point-like counterpart is significantly detected consistent with the X-ray position).

Photometry

We extracted the flux of the counterpart of HLX-1 using aperture photometry with the astrolib IDL procedure² `aper`, after centring the position of the source with the `cntrd` procedure. We used extraction radii of 0.5, 1, 1.5, 2, 2.5, 3, 4, 5, 6, 7, 8, 9, 10 pixels and subtracted the background estimated in an annulus around the source (10 to 15 pixels). The level of the background was adjusted in order to obtain a flux vs. aperture radius relation that reaches a plateau at large radii, which correspond to the total background subtracted flux of the source. This ensures that we included all the flux from the source in the aperture and that the background is correctly estimated and subtracted.

We converted the fluxes into AB magnitude using the magnitude zero points given in the HST WFC3 and ACS documentation and webpages^{3,4}. We processed

² <http://idlastro.gsfc.nasa.gov>

³ http://www.stsci.edu/hst/wfc3/phot_zp_lbn

⁴ <http://www.stsci.edu/hst/acs/analysis/zeropoints>

the WFC3/IR F160W image differently as the galaxy emission is higher in this band (10 times the flux of the counterpart of HLX-1) and needed to be subtracted. We used a clean nearby region to estimate the contribution of the galaxy at the position of HLX-1. The image was shifted by 10 pixels and then subtracted from the initial image, so as to obtain a flat background in a 6 pixels region around HLX-1. We then applied the same aperture photometry extraction procedure with smaller radii (0.5, 1, 1.5, 2, 2.5, 3, 4, 5 pixels and background in an 5 to 6 pixels annulus). Errors on the photometry were computed with the `aper` procedure as the quadratic sum of the scatter in background values, the random photon noise, and the uncertainty in mean sky brightness. The photometry for each filter is given in the log of observations in Table S1. The fluxes and errors were then converted into units of photons $\text{cm}^{-2} \text{s}^{-1}$ and XSPEC-readable spectral files (with diagonalised response files) were generated using the FTOOLS task `flx2xspec`.

Swift Data Reduction

The field of HLX-1 was observed contemporaneously with our *HST* observations with the *Swift* XRT (obsid: 00031287055, 00031287056, 00031287057, 00031287058, and 00031287059) on September 13, 14, and 23 for a total of 17.5 ks. The data were processed with the *Swift* XRT pipeline⁵ version 0.12.4. We used the grade 0-12 events, giving slightly higher effective area at higher energies than grade 0 events. A source spectrum was extracted from a circular region with a radius of 47.2" (20 pixels) centred on the position of HLX-1 using XSELECT v2.4a, while a background extraction region was chosen in a nearby source-free region of

⁵ <http://heasarc.gsfc.nasa.gov/docs/swift/analysis>

the field. Ancillary response and exposure map files were created using XRTMKARF v0.5.6 and XRTEXPOMAP v0.2.7 respectively, while the response file swxpc0to12s6_20070901v011.rmf was used in the spectral fitting process. The spectra were binned to a minimum of 20 counts per bin in order to use χ^2 statistics for the fitting.

SED Fitting

The SED fitting to the *HST* and *Swift* data was performed in XSPEC v12.6.0q. The *Swift* XRT data were consistent with both multi-colour disc black body and power law models, although recent *Chandra* observations indicated it was in the high/soft state with an X-ray spectrum dominated by thermal disc emission (12). We therefore first fitted the *HST* and *Swift* data contemporaneously with a multi-coloured disc black body model (DISKBB), with the addition of absorption (using the TBABS model and the elemental abundances prescribed in (29)) and extinction components (using the REDDEN model) representing absorption by the neutral hydrogen column and dust reddening, respectively. Although this model accounts for the X-ray emission very nicely, we could not obtain an acceptable fit to the *HST* data ($\chi^2/dof = 137.54/33$), with the fit residuals indicating the presence of a strong red-excess in the SED.

We next tried fitting the SED with the DISKIR model representing emission from an irradiated accretion disc (30). Unlike the simple DISKBB model, the irradiated disc model accounts for emission from the inverse Compton tail as well as emission arising from irradiation of the outer disc. As the X-ray spectrum is dominated by the thermal component with no significant evidence of any Compton tail, we fixed the slope of the Compton tail to a value of 2.1, consistent with

previous observations of HLX-1 in the high/soft spectral state (12). As with the previous simple model, fitting the SED with an irradiated disc model described the X-ray part of the spectrum well, but not the *HST* data ($\chi^2/dof = 55.11/28$).

The position of HLX-1 ~ 1 kpc out of the plane of ESO 243-49 is easy to explain if the black hole were embedded in a cluster of stars, either a globular cluster or the remnant of a nucleated dwarf galaxy. We therefore attempted to fit the red excess in the SED using stellar population models. We generated XSPEC additive table models for the Maraston (2005) stellar population models based on theoretical atmospheres with the Salpeter initial mass function, using the FTOOLS routine WFTBMD. These models have 4 variable parameters: metallicity ($0.2 - 2 Z_{\odot}$), Age ($1 \times 10^6 - 2 \times 10^9$ yr), redshift and normalisation. We thus added a stellar population component to the absorbed, reddened, irradiated disc model with the redshift frozen at the value of $z = 0.0223$ obtained from VLT spectroscopy (Wiersema et al. 2010) but with the remaining parameters free to vary. An excellent fit was obtained with this irradiated disc plus stellar population model ($\chi^2/dof = 29.03/27$), with a stellar population with a mass of $\sim 4 \times 10^5 M_{\odot}$ and moderate irradiation of the outer accretion disc ($f_{out} \sim 1 \times 10^{-3}$). However, when attempting to determine uncertainties on the fit parameters, XSPEC found a slightly better fit ($\chi^2/dof = 25.18/27$) with essentially no outer disc irradiation ($f_{out} \sim 2 \times 10^{-5}$) and a higher stellar mass of $\sim 2 \times 10^6 M_{\odot}$. Both fit solutions are statistically acceptable, and we cannot discriminate between the two due to degeneracies in the model fitting. The metallicity of the stellar population could not be constrained in either solution, with the value hitting the hard upper limit of the model at $Z = 2 Z_{\odot}$. Likewise, the upper limit to the outer disc radius could not be accurately constrained. However, the modelling found that the SED was not consistent with an

old stellar population, instead obtaining an age of ~ 6 Myr in both cases. Table 1 lists the best-fit spectral parameters for the minimal irradiation solution, while Figures 2 and 3 show the SED fit with this same model and the unabsorbed/de-reddened model, respectively.

To test for model dependency in the fit, we also generated additive table models using stellar population models based on empirical stellar libraries by (20). In particular, we used the models based on the Pickles (31) Solar metallicity library, because of their extended wavelength range. Replacing the theoretical atmosphere models with these empirical stellar library models also obtained an excellent fit ($\chi^2/dof = 27.32/28$), with consistent model parameters albeit with a slightly older cluster age (~ 8 Myr), a lower derived luminosity ($\sim 9 \times 10^7 L_{\odot}$) and a lower mass ($\sim 5 \times 10^5 M_{\odot}$). However, once again the degree of irradiation could not be constrained, highlighting the degeneracies between the irradiation fraction and the mass (and thus luminosity) of the stellar population. It is thus clear that additional *HST* data obtained at different X-ray luminosity levels are required in order to accurately constrain both the presence of disc irradiation and the mass of the stellar population surrounding HLX-1. Significant variability in any of the *HST* bands correlated with the previously observed X-ray variability would imply that that band has a significant contribution from a reprocessed disc component, as the stellar population emission should not vary. The detection of any optical variability – particularly in the near-infrared bands – would thus provide support for the irradiated disc solution.

Table S1 Log of *HST* Observations

Instrument	Filter	Date	t_{exp} (s)	λ_{pivot} (Å)	FWHM (Å)	Magnitude (AB mag)
ACS-SBC	F140LP far-UV	2010-09-13	2480	1527	294.08	24.8 ± 0.05
WFC3-UVIS	F300X near-UV	2010-09-23	1710	2829.8	753	24.27 ± 0.02
WFC3-UVIS	F390W C-band	2010-09-23	712	3904.6	953	24.33 ± 0.03
WFC3-UVIS	F555W V-band	2010-09-23	742	5309.8	1595.1	24.16 ± 0.02
WFC3-UVIS	F775W I-band	2010-09-23	740	7733.6	1486	24.15 ± 0.1
WFC3-IR	F160W H-band	2010-09-23	806	15405.2	2878.8	24.56 ± 0.3

Table S2 Details of Astrometric Corrections

Filter	N _{ISPI}	Fit RMS	Astrometric error	
			<i>HST</i> error	Total error
F140LP	4	0.01"	0.35"	0.47"
F300X	6	0.05"	0.35"	0.47"
F390W	8	0.05"	0.35"	0.47"
F555W	18	0.09"	0.40"	0.50"
F775W	25	0.09"	0.40"	0.50"
F160W	22	0.10"	0.41"	0.50"

The F140LP image was aligned on the F300X image, which was in turn aligned on the ISPI image in a 3-step process. The *HST* astrometric errors include the UCAC3 absolute error of 0.05" and the ISPI relative error of 0.13" (1σ). The total errors include the 0.3" X-ray position error as measured with *Chandra* (Webb et al. 2010). All errors quoted in the table are at the 95% significance level.